fluids

MDPI

Article

Enhancement of PEMFC Performance Using Symmetric V-Tapered Flow Channels

Mohamed El Amine Guerbazi [1], Adel Chine [1], Fouad Khaldi [1], Abdallah Mohammedi [2], Alaeddine Zereg [3] and Nadhir Lebaal [3,4,*]

[1] LEREESI Laboratory, HNS-RE2SD, Batna 05078, Algeria; me.guerbazi@hns-re2sd.dz (M.E.A.G.); a.chine@hns-re2sd.dz (A.C.); fouad.khaldi@hns-re2sd.dz (F.K.)
[2] Laboratory of Advanced Materials Technology, Ecole Nationale Polytechnique de Constantine, Nouvelle Ville RP, B.P. Box 75, Constantine 25000, Algeria; abdallah.mohammedi@gmec.enp-constantine.dz
[3] Laboratoire Interdisciplinaire Carnot de Bourgogne (ICB), UMR CNRS 6303, Université Marie et Louis Pasteur, UTBM, 90010 Belfort, France; alaeddine.zereg@utbm.fr
[4] Laboratoire Interdisciplinaire Carnot de Bourgogne (ICB), UMR CNRS 6303, Université Bourgogne Europe, 21000 Dijon, France
* Correspondence: nadhir.lebaal@utbm.fr

Abstract

This study presents an optimized symmetric V-tapered cross-section (SVTC) flow-field geometry for a single-channel Proton Exchange Membrane Fuel Cell (PEMFC). Its performance is evaluated through three-dimensional Computational Fluid Dynamics (CFD) simulations conducted using ANSYS FLUENT 18.1. The SVTC architecture incorporates angled sidewalls that progressively taper the channel width, aiming to accelerate mass diffusion and increase reactant effectiveness in the cell. Performance metrics including current density, pressure drop, and net power output were analyzed across six SVTC configurations with varying taper ratios. Comparative evaluation with a conventional rectangular channel indicates that the SVTC design enhances the hydrogen and oxygen distribution, improves water management, and reduces mass transport losses. Specifically, the R5 configuration exhibited the most favorable results, achieving a peak net power density of 0.297031 W/cm^2 while reducing the pressure drop by approximately 21% relative to the R1 configuration. Furthermore, the SVTC configuration enhance both current density and power density, demonstrating its effectiveness in improving mass transport and overall cell performance. The design also demonstrated improved reactant distribution uniformity and operational stability across varying load conditions. These findings underscore the critical role of channel geometry in PEMFC performance and highlight the potential of SVTC designs to enable more efficient and scalable fuel cell systems through targeted geometric optimization.

Keywords: CFD; PEMFC; SVTC; power produced; pressure drop; taper ratio

check for updates

Academic Editor: Wenning Zhou

Received: 24 September 2025
Revised: 25 November 2025
Accepted: 25 November 2025
Published: 30 November 2025

Citation: Guerbazi, M.E.A.; Chine, A.; Khaldi, F.; Mohammedi, A.; Zereg, A.; Lebaal, N. Enhancement of PEMFC Performance Using Symmetric V-Tapered Flow Channels. *Fluids* **2025**, *10*, 315. https://doi.org/10.3390/fluids10120315

Copyright: © 2025 by the authors. Licensee MDPI, Basel, Switzerland. This article is an open access article distributed under the terms and conditions of the Creative Commons Attribution (CC BY) license (https://creativecommons.org/licenses/by/4.0/).

1. Introduction

Owing to escalating environmental concerns, the demand for clean energy solutions has seen a substantial rise [1–3]. Hydrogen energy offers substantial promise in advancing the transition to a clean energy future and plays a crucial role in achieving deep decarbonization on a large scale. Water electrolysis represents a pivotal technology for green hydrogen production, offering a sustainable pathway to generate hydrogen while simultaneously mitigating the intermittency and variability inherent in renewable energy

sources, thereby enhancing grid stability and energy storage capabilities [4,5]. Fuel cells, particularly PEMFC, have emerged as a promising technology in this shift. A fuel cell operates by reacting hydrogen with oxygen to form water and release heat, while the associated electrochemical process produces electrical power [6]. Their low-temperature operation, fast start-up capabilities, and strong energy-conversion performance make these fuel cells attractive for portable power devices, transportation technologies, and various co- or multigeneration applications [7]. Previous studies emphasize that the geometry of the flow channels within the bipolar plates is a crucial factor, as well-designed channels enhance mass transport and can substantially raise the achievable power density of PEMFC systems [8].

Recognizing the significant influence of channel architecture on PEMFC performance, extensive numerical and experimental investigations have been devoted to examining both traditional channel configurations and emerging, non-conventional flow-path concepts. Many recent designs introduce internal features or adopt biomimetic structural ideas to lower pressure losses between the inlet and outlet passages, ultimately improving overall cell performance. Kumar and Reddy [9] examined four distinct flow-field layouts serpentine, parallel, multi-parallel, and discontinuous under both steady-state and transient operating conditions. They found that the discontinuous configuration offered superior power density during steady operation, whereas parallel-type channels delivered better performance when the system underwent transient changes. Kuo and Chen [10] proposed a wavy-shaped channel configuration that increased convective heat transfer, which in turn accelerated electrochemical reaction rates and improved cell output, particularly under high current density conditions. Drawing inspiration from the branching structure of the mammalian lung, Kloess et al. [11] designed a biomimetic flow field that produced markedly more uniform gas distribution, as demonstrated through numerical simulation. Xiao et al. [12] carried out numerical development of a PEMFC model inspired by the vein network of a tree leaf, providing theoretical justification for the optimization of such biomimetic flow-field architectures.

CFD has become an indispensable approach for investigating and optimizing the performance of PEMFCs. Numerical simulations provide detailed insights into local flow patterns, species transport, and electrochemical interactions that are often difficult to capture experimentally. Recent studies have demonstrated that CFD enables systematic evaluation of channel geometry, taper ratios, and operating conditions, offering predictive capabilities for fuel distribution, water management, and pressure loss estimation. This approach not only reduces experimental costs and development time but also provides valuable guidance for improving flow field design and enhancing overall system efficiency [13–15].

Moreover, recent CFD investigations [16–20] have demonstrated remarkable progress in predictive modeling and simulation accuracy. These developments further establish CFD as a crucial tool for analyzing complex thermo-fluid dynamics and optimizing advanced energy systems such as PEM fuel cells.

Several researchers have investigated the geometric effects on PEMFC performance. Karrar H. Fahim et al. [21] emphasized that flow field geometry is critical in achieving uniform reactant distribution across the catalyst surface, thereby enhancing electrochemical reactions and overall fuel cell efficiency. Elena Carcadea et al. [22] conducted CFD and experimental analyses of various serpentine flow field configurations. Their findings revealed that increasing the number of channels and reducing channel width, particularly in a 14-channel layout, led to improved water management and higher current density, especially at elevated loads.

Additional studies have explored global geometric variables such as parallel-serpentine designs, mesh configurations, and tubular channel structures. Leila Rostami et al. [23] proposed a novel V-Ribbed flow field design that merges serpentine and parallel characteristics to enhance gas distribution and reduce pressure drop. Their CFD results showed improved oxygen transport, reduced liquid water accumulation, and up to a 41.5% increase in current density compared to traditional designs. Similarly, Feng Sun et al. [24] developed a 3D fine-mesh flow field model and demonstrated that increasing the porosity of the structure enhanced oxygen availability and reduced pressure losses, resulting in a 21.5% increase in peak power density over conventional parallel designs. Lastly, Lei Yuan et al. [25] investigated tubular PEMFC with different flow arrangements and found that counter-flow configurations, particularly the square chordal design, significantly improved reactant uniformity and net power output.

Numerous investigators have demonstrated that the shape of the flow path and cross-section in PEMFC channels plays a crucial role in enhancing cell performance. Elaibi et al. [26] investigates the impact of novel mixed cross-sectional flow-channel designs on fuel cell performance. The study concludes that these designs improve efficiency, reliability, and contribute to advancing clean energy technologies. Similarly, Wang et al. [27] developed a variable cross-section wavy flow channel for PEM fuel cells to enhance mass transfer and water removal efficiency. Their CFD simulations identified optimal geometric parameters that improved current density by 9.06% compared to conventional designs.

Mahmut Kaplan et al. [28] developed a 3D model showing that reducing channel width and depth significantly enhances current density (up to 57%) due to increased gas velocity, though at the cost of higher pressure drop. Keke Liu et al. [8] proposed dome-like and branched variable cross-section channels, with CN-19 achieving the best performance, increasing current and power densities by enhancing oxygen distribution and flow. Chakrit Suvanjumrat et al. [29] used a 3D multiphase CFD model to find that a channel aspect ratio of 1.0 maximizes power density, balancing pressure drop and transport efficiency. Yi Wu et al. [30] compared five channel shapes rectangular, triangular, trapezoidal, inverted trapezoidal, and elliptical and reported that the triangular channel achieved the best performance in high-temperature PEMFCs by enhancing reactant utilization and gas permeation.

While existing research has explored either tapered channels (to accelerate flow and compensate for reactant depletion) or V-shaped cross-sections (to enhance under-rib convection), these approaches are often treated in isolation. The critical research gap lies in creating a synergistic design that effectively integrates both strategies. This study introduces the novel SVTC, an architecture specifically engineered to address this challenge. The SVTC is a multifunctional design. Its angled “V” walls are configured to promote under-rib convection, while its progressive symmetric tapering is designed to simultaneously accelerate flow, maintaining high reactant concentration and optimizing mass transport along the entire channel. This work moves beyond simple geometric comparisons to investigate the specific influence of these combined design parameters. By evaluating multiple SVTC configurations against traditional rectangular channels, this study demonstrates a new, integrated approach to flow field design, proving that the synergy of these features leads to significant enhancements in power density and vapor water management.

2. Numerical Method and Model Setup

2.1. Geometric Configuration

This study investigates a single-channel PEMFC with straight gas channels and a planar flow field design. The geometrical models of the selected PEMFC configurations were developed using ANSYS Design Modeler, as illustrated in Figure 1a,b.

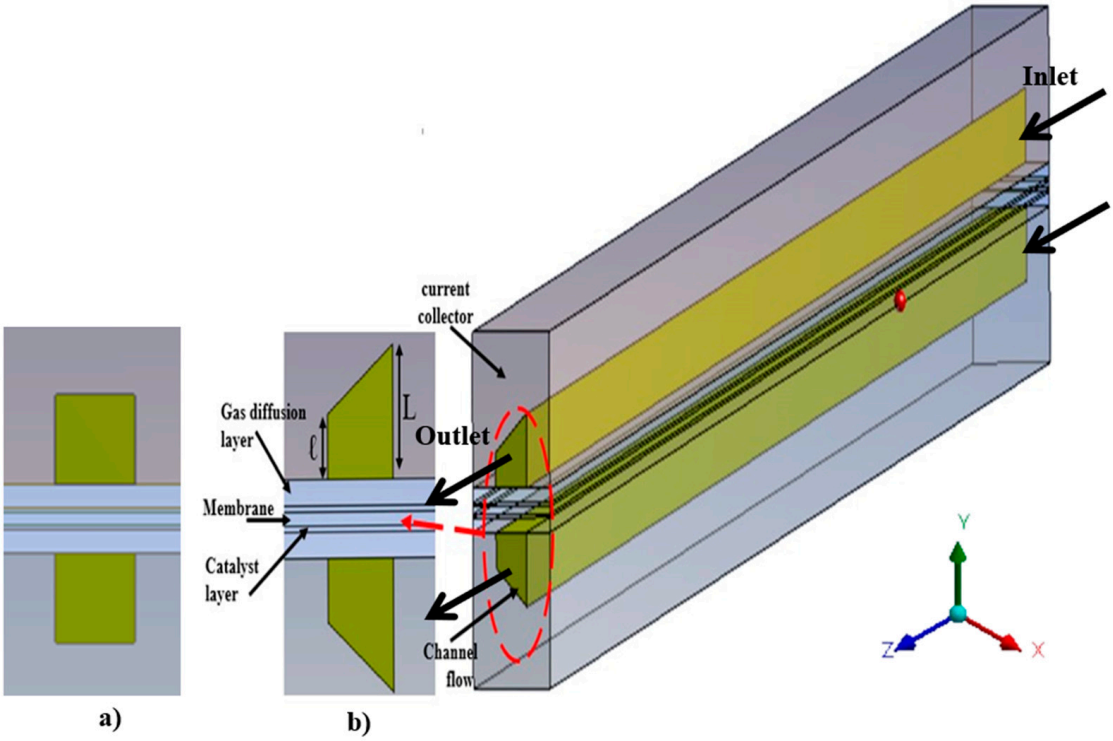


Figure 1. Geometric configurations of the studied PEMFC flow channels: (**a**) Conventional rectangular channel and (**b**) SVTC channel.

The cell structure consists of a current collector, a gas flow channel, a gas diffusion layer (GDL), and a catalyst layer (CL) on both the anode and cathode sides. A membrane is centrally positioned between these layers, forming a complete layered assembly. The detailed dimensions of each component are presented in Table 1.

Table 1. Geometric parameters.

Parameters	Units	Dimensions
Cell length	Mm	100
Channel width	Mm	0.8
Membrane thickness	Mm	0.1
Catalyst layer thickness	Mm	0.048
Gas diffusion layer thickness	Mm	0.2

For the SVTC design, the trapezoidal channel section is characterized by lower and upper base lengths, denoted as ℓ and L, respectively, where ℓ < L, as shown in Figure 1b. The ratio R = ℓ /L is introduced as a key geometric design parameter and is systematically varied to assess and optimize cell performance, as shown in Table 2.

Table 2. SVTC channel base ratio configurations.

Symbol	ℓ Shorter Base (mm)	L Longer Base (mm)	R = ℓ /L	Note
R1	0.20	1.28	0.156	Lowest ratio
R2	0.30	1.18	0.254	
R3	0.40	1.08	0.370	
R0	0.48	1.00	0.480	Reference value
R4	0.50	0.98	0.510	
R5	0.60	0.88	0.682	Highest in this range

The simulation is conducted based on the following set of assumptions:

- The model operates under steady-state and non-isothermal conditions.
- Fluid flow is assumed to be laminar and incompressible.
- The GDL, CL, and membrane are modeled as isotropic and homogeneous porous media.
- Reactive gases follow ideal gas behavior.
- Liquid water formation is neglected, and only water vapor transport is considered.

2.2. Modeling and Simulation Approach

In this study, two channel cross-sectional geometries SVTC and rectangular were analyzed using the ANSYS FLUENT 18.1 [31] CFD software, as illustrated in Figure 1. The symmetric V-tapered channel, characterized by a straight main path with opposing angled indentations forming a "V" shape on both the upper and lower walls, is designed to enhance local turbulence and improve reactant distribution across the flow field.

Numerical simulations are employed to evaluate how these channel configurations affect the fuel cell's performance, pressure distribution, and transport phenomena within the PEMFC. The three-dimensional simulation framework integrates the Navier–Stokes equations for fluid flow, along with governing equations for energy and mass conservation, species transport, electrical charge conservation, and electrochemical kinetics described by the Butler-Volmer equation. The formulation and implementation of the coupled physical models follow the methodologies provided in the ANSYS PEMFC Add-on Module [27,28].

- Conservation of mass

$$\frac{\partial(\rho u)}{\partial x} + \frac{\partial(\rho v)}{\partial y} + \frac{\partial(\rho w)}{\partial z} = S_m = 0 \tag{1}$$

- Conservation of momentum

$$u\frac{\partial(\rho u)}{\partial x} + v\frac{\partial(\rho u)}{\partial y} + w\frac{\partial(\rho u)}{\partial z} = -\frac{\partial P}{\partial x} + \frac{\partial}{\partial x}\left(\mu_{eff}\frac{\partial u}{\partial x}\right) + \frac{\partial}{\partial y}\left(\mu_{eff}\frac{\partial u}{\partial y}\right) + \frac{\partial}{\partial z}\left(\mu_{eff}\frac{\partial u}{\partial z}\right) + S_x \tag{2}$$

$$u\frac{\partial(\rho v)}{\partial x} + v\frac{\partial(\rho v)}{\partial y} + w\frac{\partial(\rho v)}{\partial z} = -\frac{\partial P}{\partial y} + \frac{\partial}{\partial x}\left(\mu_{eff}\frac{\partial v}{\partial x}\right) + \frac{\partial}{\partial y}\left(\mu_{eff}\frac{\partial v}{\partial y}\right) + \frac{\partial}{\partial z}\left(\mu_{eff}\frac{\partial v}{\partial z}\right) + S_y \tag{3}$$

$$u\frac{\partial(\rho w)}{\partial x} + v\frac{\partial(\rho w)}{\partial y} + w\frac{\partial(\rho w)}{\partial z} = -\frac{\partial P}{\partial z} + \frac{\partial}{\partial x}\left(\mu_{eff}\frac{\partial w}{\partial x}\right) + \frac{\partial}{\partial y}\left(\mu_{eff}\frac{\partial w}{\partial y}\right) + \frac{\partial}{\partial z}\left(\mu_{eff}\frac{\partial w}{\partial z}\right) + S_z \tag{4}$$

Variables u, v, and w denote the velocity components along the x, y, and z axes, respectively.

$$S_x = -\left(\frac{\mu u}{k_x}\right) \tag{5}$$

$$S_y = -\left(\frac{\mu v}{k_y}\right) \tag{6}$$

$$S_z = -\left(\frac{\mu w}{k_z}\right) \tag{7}$$

In this formulation, the symbol μ represents the dynamic viscosity of the gas phase, while k_x, k_y, and k_z denote the directional permeability components in the x, y, and z directions, respectively, for both the CL and GDL.

Energy Transport

The conservation of energy is described by:

$$u\frac{\partial(\rho C_p T)}{\partial x} + v\frac{\partial(\rho C_p T)}{\partial y} + w\frac{\partial(\rho C_p T)}{\partial z} = \frac{\partial}{\partial x}\left(k_{eff}\frac{\partial T}{\partial x}\right) + \frac{\partial}{\partial y}\left(k_{eff}\frac{\partial T}{\partial y}\right) + \frac{\partial}{\partial z}\left(k_{eff}\frac{\partial T}{\partial z}\right) + S_h \tag{8}$$

- Species transfer

$$u\frac{\partial \rho y_i}{\partial x} + v\frac{\partial \rho y_i}{\partial y} + w\frac{\partial \rho y_i}{\partial z} = \frac{\partial}{\partial x}\left(\rho D_i\frac{\partial y_i}{\partial x}\right) + \frac{\partial}{\partial y}\left(\rho D_i\frac{\partial y_i}{\partial y}\right) + \frac{\partial}{\partial y}\left(\rho D_i\frac{\partial y_i}{\partial y}\right) + S_i \tag{9}$$

- Cell potential

While a fuel cell's maximum theoretical voltage is defined by its thermodynamic equilibrium potential (E), the actual operating voltage is always lower due to irreversible losses that occur when current is drawn. The usable cell potential (V_{cell}) is therefore determined by deducting the sum of all voltage losses, or overpotentials, from this ideal potential, as given by the following relationship [26]:

$$E_{cell} = E - \eta_{ohm} - \eta_{mem} - \eta_{Diff} \tag{10}$$

- Activation Overpotential

The activation overpotential, denoted as $\eta a, c[V]$ are determined from the local electrical potentials in the electrodes and membrane [27]:

$$\eta_{a,c} = E_r - ir - \eta_{mem} - V_{input,cat} \tag{11}$$

where η_{ohm} represents the ohmic losses. The parameter V_{cat} corresponds to the cathode half-cell potential, which serves as a model input to establish the operating condition of the fuel cell. The reversible cell potential E in Equation (11) is obtained from the In Proceedings of the Nernst equation [23]:

$$E = 1.23 - 0.9 \times 10^{-3}(T - 298) + 4.3085 \times 10^{-5} T \times \left[\ln P_{H_2} + 1/2 \ln P_{O_2}\right] \tag{12}$$

The ohmic losses in Equation (11) are computed by solving the potential distribution equations within the gas diffusion layers.

- Membrane ancillary

The polymer electrolyte membrane plays a key role in understanding water transport behavior within fuel cells. Inside the membrane, water moves through two main mechanisms electro-osmotic drag and diffusion both of which are governed by the membrane's hydration level. The corresponding protonic conductivity, σ, is determined using the empirical relation provided in Refs. [27,29]:

$$\sigma_{mem} = (0.00514\lambda - 0.00326)e^{1268(\frac{1}{303}-\frac{1}{T})} \quad (13)$$

The above empirical expression for membrane protonic conductivity follows the correlation proposed by Springer et al. [32] for Nafion 117 membranes. In this relation, λ is the number of water molecules per sulfonic acid group (dimensionless) and T is the absolute temperature (K). The constants were empirically adjusted to yield conductivity in $ohm^{-1}\ m^{-1}$, ensuring full dimensional consistency. This formulation remains the standard model for describing the coupled influence of temperature and hydration on proton transport in polymer electrolyte membranes.

2.3. Boundary Conditions

All simulations maintained constant flow rates at the channel inlets, consistent with the specified anode and cathode humidification levels, using air as the oxidant. Dirichlet boundary conditions were imposed on species concentration, heat, and mass flow at the anode and cathode inlets, while the outlets were governed by a specified pressure. The external surfaces of the fuel cell were treated with Neumann boundary conditions to ensure zero flux and adiabatic walls. The transport equations for species, momentum, energy, mass, electric charges, and electrochemical kinetics were solved using the software's integrated algorithm. To ensure numerical stability, relaxation coefficients of 0.95 were applied to the species, water content, and energy equations, with coefficients of 0.3 and 0.7 used for momentum and pressure, respectively. The solver utilized F-cycle Multigrid cycles (Full Approximation Scheme) to accelerate convergence, and the BICGSTAB method (Biconjugate Gradient Stabilize Method) was employed to stabilize the iterative solutions for species concentrations, water saturation, and electrical potentials. The cell's performance was evaluated by constructing a polarization (I–V) curve from 160 steady-state simulations, sweeping the voltage from an open circuit condition down to 0.15 V.

2.4. Mesh Independence

A mesh independence study was conducted to evaluate the numerical uncertainty associated with the spatial discretization in the CFD model. Using ANSYS Mesh, five distinct non-uniform grids were generated, refined in the x- and y-directions while maintaining a uniform structure in the z-direction.

The resulting polarization curves for all five cases, shown in Figure 2, demonstrated very close agreement. The mesh comprising 36,000 elements was selected for all subsequent simulations, as its I-V curve occupied a central position among the tested cases, confirming its representativeness. This configuration offers an optimal balance, being the smallest mesh that substantially reduces computational expense without compromising result accuracy.

The finalized mesh structure featured 80 divisions along the Z-axis, 10 along the x-axis, and a y-axis distribution of five divisions each for the CL, GDL, and membrane, 10 for the current collector, and five for the channel.

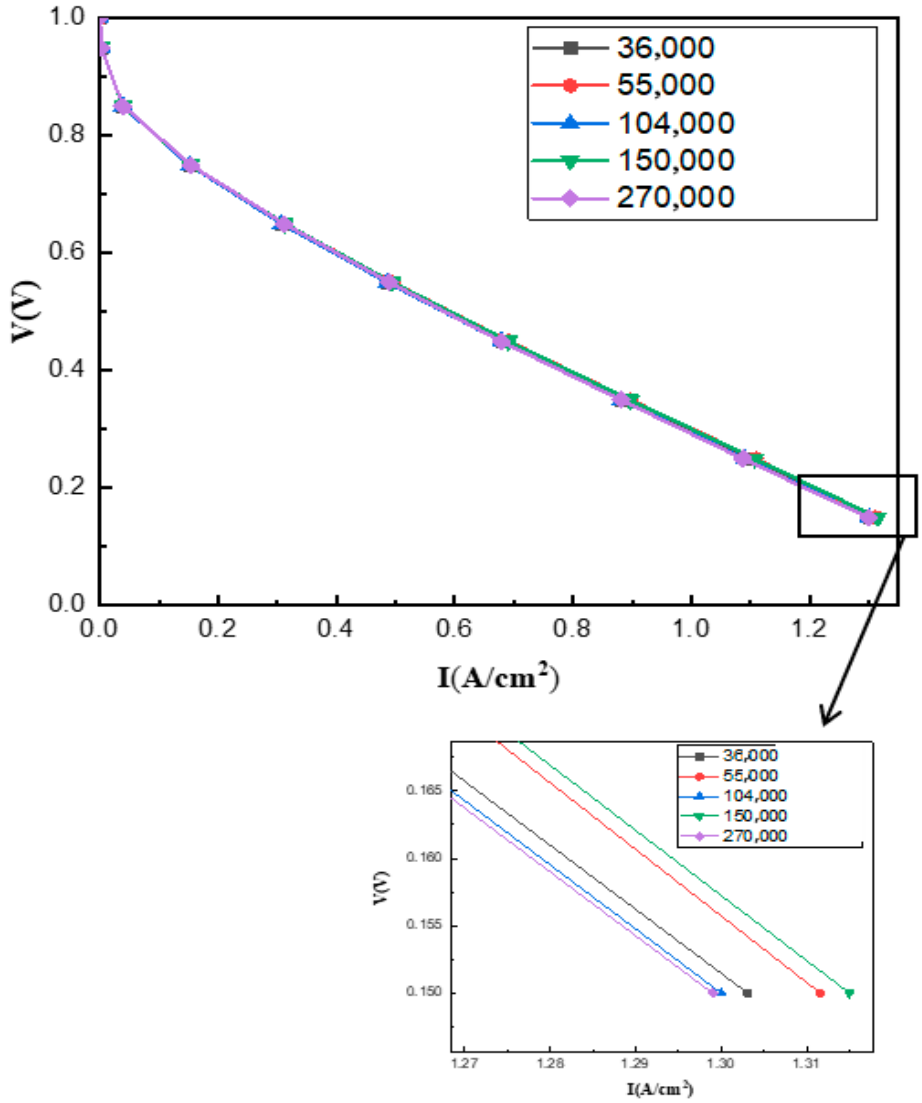


Figure 2. Mesh independence analysis.

2.5. Validation

The accuracy of the computational model was verified by comparing the simulated polarization curve with published experimental results from Ticianelli et al. [33], as presented in Figure 3.

The model demonstrates excellent agreement with the experimental results in the low current density region, confirming its predictive accuracy under these conditions. A minor deviation emerges at higher current densities, where the simulated voltage slightly overpredicts the experimental values. This discrepancy is likely due to factors such as mass transport overpotentials, inherent model simplifications, or unaccounted thermal effects that become more pronounced at high loads.

Nevertheless, with a mean absolute percentage error of 6% across the operating range, the validation confirms that the simulation robustly captures the overall performance characteristics of the PEMFC, affirming its suitability for the present study.

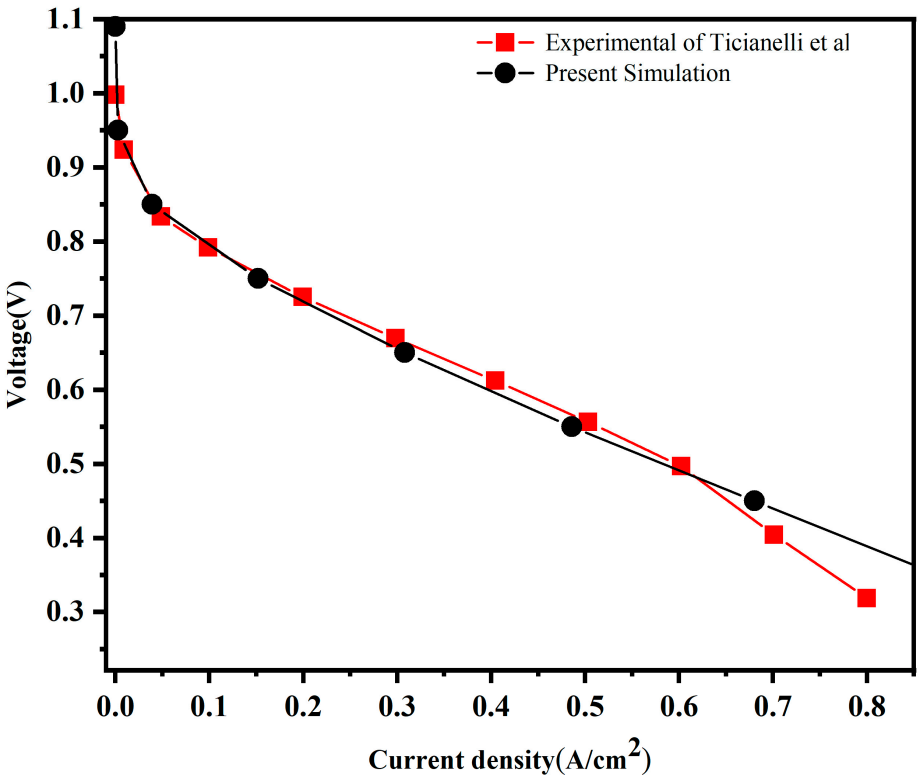


Figure 3. Validation of the numerical model against the experimental polarization data reported by Ticianelli et al. [33].

3. Results and Discussion

After developing and simulating a PEMFC single-cell base model featuring straight channels in the commercial CFD software ANSYS FLUENT 18.1 [31], Our earlier studies [34,35] comprehensively address the mesh independence test and offer a detailed comparison between numerical simulations and experimental data. While these referenced articles contain extensive information and analysis, this study also includes a validation figure for completeness.

Two comparison strategies are employed in this study to evaluate the influence of channel geometry on fuel cell performance:

1. Shape-based comparison: The first strategy involves comparing a conventional rectangular channel (with dimensions ℓ = L = 0.8 mm) to the proposed SVTC geometry. In this case, both the cross-sectional area and the channel height are kept constant, allowing a direct assessment of the impact of geometry shape alone.
2. Taper ratio-based comparison: The second strategy uses a tapered reference channel Here, the taper ratio R = ℓ /L is systematically varied. To ensure a fair comparison, the cross-sectional area is held constant by adjusting the channel length L according to changes in ℓ. This method isolates the effect of tapering from variations in the inlet area, enabling a more precise evaluation of taper geometry on performance.

3.1. Effect of Cross-Section Geometry

The results presented in Figures 4 and 5 clearly demonstrate the superior performance of the SVTC design compared to the rectangular channel configuration in a PEMFC.

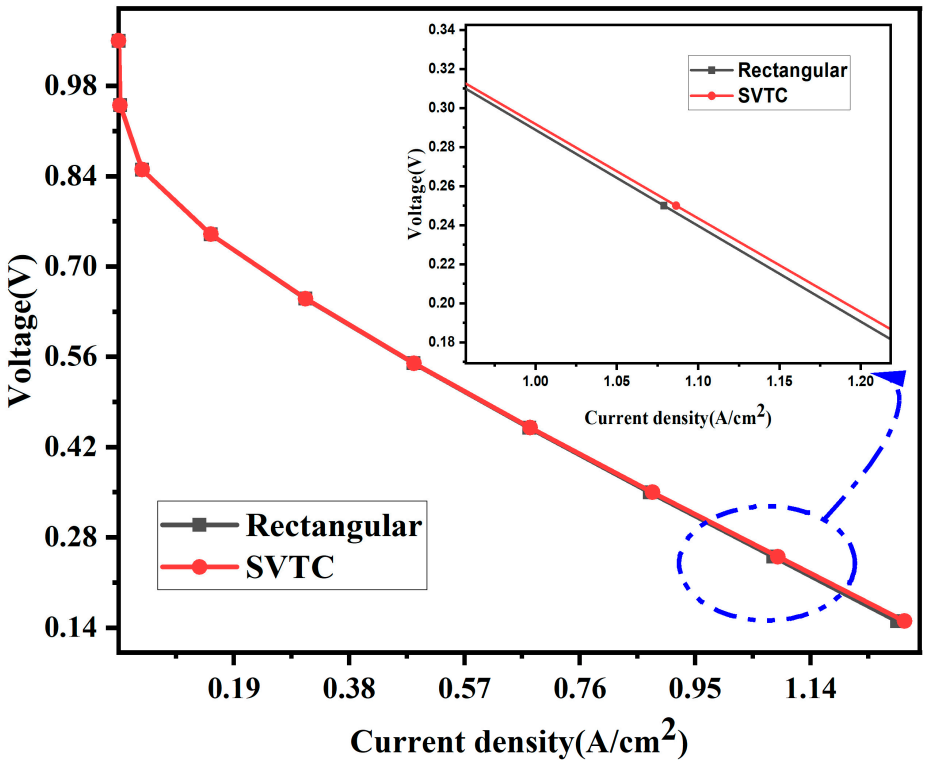


Figure 4. Polarization curve comparison: rectangular vs. SVTC channels.

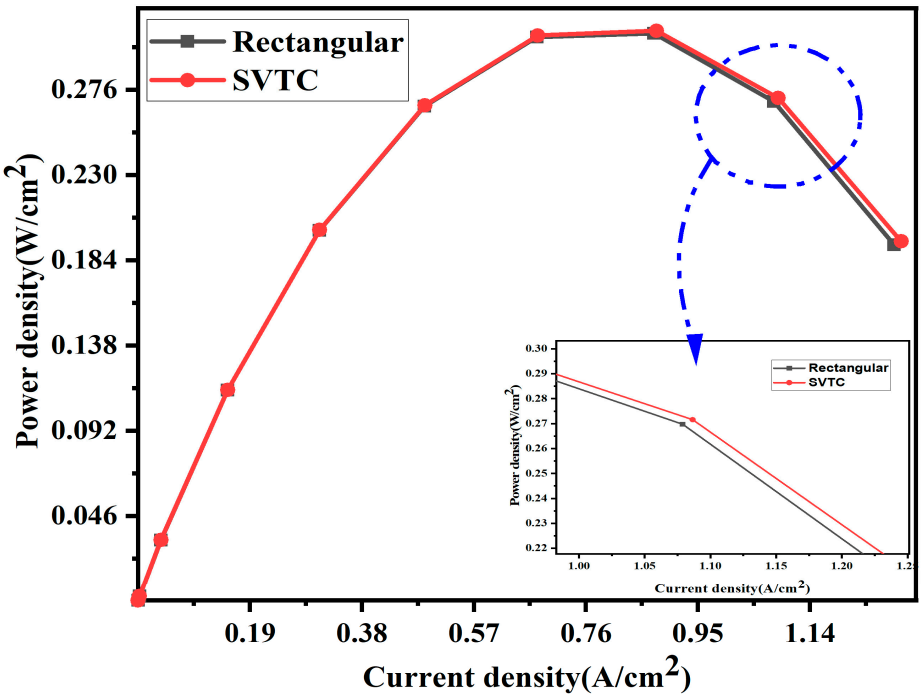


Figure 5. Comparative power density characteristics of rectangular and SVTC channels.

An analysis of the polarization curves in Figure 4 reveals enhanced voltage stability in the SVTC channel configuration relative to the conventional rectangular design. The SVTC maintains a higher voltage at elevated current densities, suggesting a reduction in both activation and ohmic losses. At a cell voltage of 0.35 V, the rectangular channel delivers a current density of 0.8755 A/cm^2, whereas the SVTC reaches 0.8796 A/cm^2. This improvement is attributed to more effective reactant transport and enhanced electrochemical activity within the flow field.

As shown in Figure 5, the comparison of power density curves clearly demonstrates the superior performance of the SVTC channel configuration compared to the conventional rectangular design. The SVTC achieves a higher peak power output, suggesting more efficient fuel utilization and enhanced water and gas management within the flow field. At a cell voltage of 0.35 V, the rectangular channel produces a power density of 0.306425 W/cm^2, whereas the SVTC yields 0.30786 W/cm^2. Although the difference is modest, the consistent improvement underscores the influence of channel geometry on overall output efficiency.

These findings affirm that structural optimization particularly in channel geometry plays a pivotal role in enhancing fuel cell performance and improving overall operational efficiency.

Figure 6 shows the hydrogen mass fraction distribution in the anode channels. The SVTC design exhibits a uniform hydrogen distribution throughout the flow field, unlike the rectangular channel, which shows significant depletion near the outlet regions. Such fuel starvation zones in the rectangular design directly contribute to the drop in voltage seen in Figure 4.

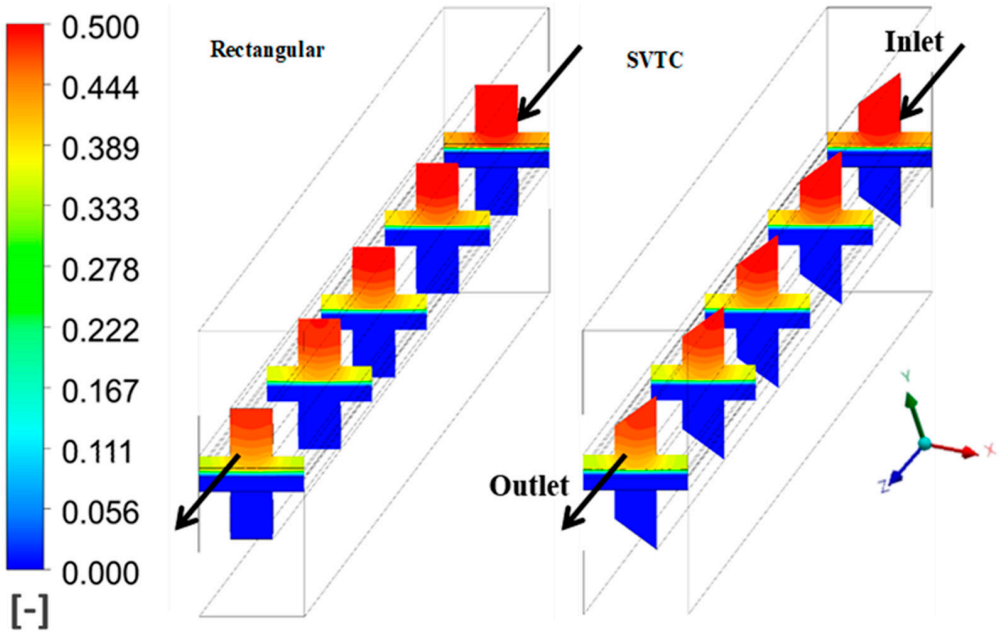


Figure 6. Comparative distribution of hydrogen mass fraction in anode channels for rectangular and SVTC designs (mass fraction, dimensionless).

Figure 7 presents the oxygen molar concentration in the cathode channels. In the SVTC configuration, oxygen is more evenly distributed, enabling efficient reduction reactions across the active surface area. In contrast, the rectangular design exhibits oxygen starvation regions, especially at the downstream ends, leading to reduced reaction rates and a more pronounced voltage loss at higher current densities.

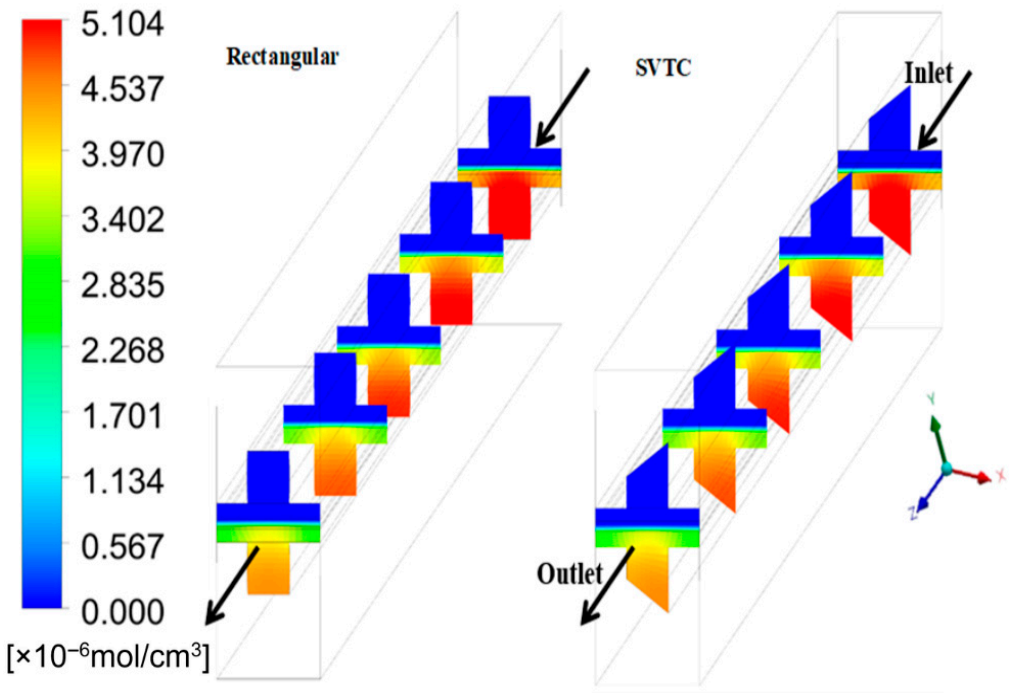


Figure 7. Comparative distribution of oxygen molar concentration in cathode channels for rectangular and SVTC designs.

Figure 8 displays the water molar concentration within the cell. The SVTC design ensures effective water removal, avoiding accumulation and flooding that can block reactant access. Meanwhile, the rectangular design is prone to water buildup, especially in low-velocity corners, which increases mass transport limitations and negatively affects power output as seen in Figure 5.

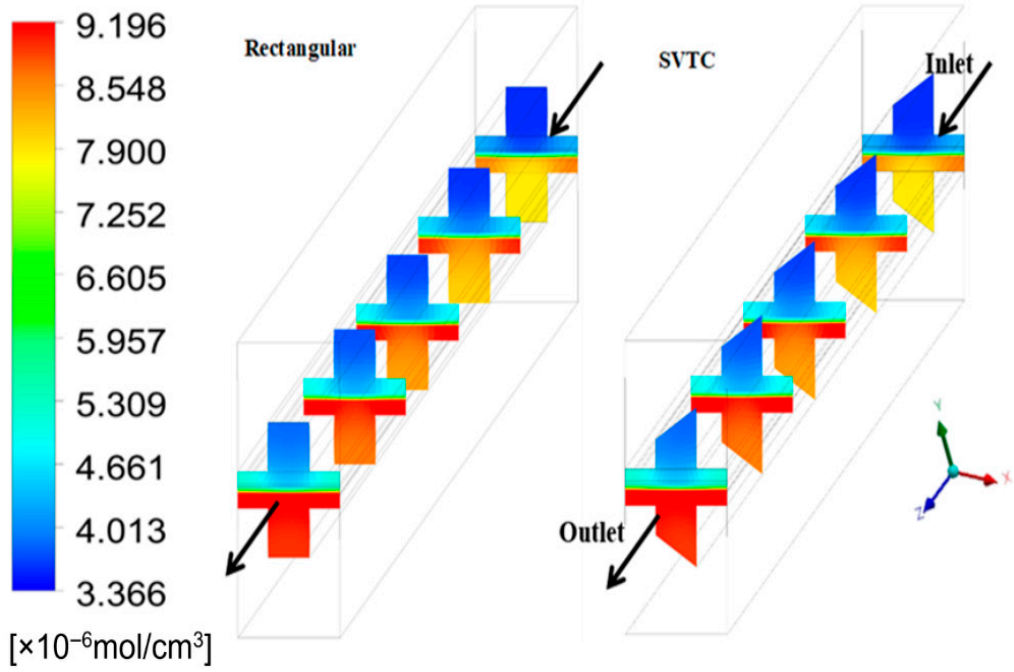


Figure 8. Comparative distribution of water molar concentration in PEMFC for rectangular and SVTC designs.

Figure 9 displays the temperature distribution within the PEMFC for rectangular and SVTC designs. The SVTC configuration shows slightly higher temperature values, particularly near the outlet, due to enhanced electrochemical reactions and improved reactant diffusion along the tapered sidewalls. This moderate temperature rise promotes better proton conductivity and more uniform heat distribution, while the rectangular design exhibits cooler zones caused by uneven reactant transport and localized reaction intensity.

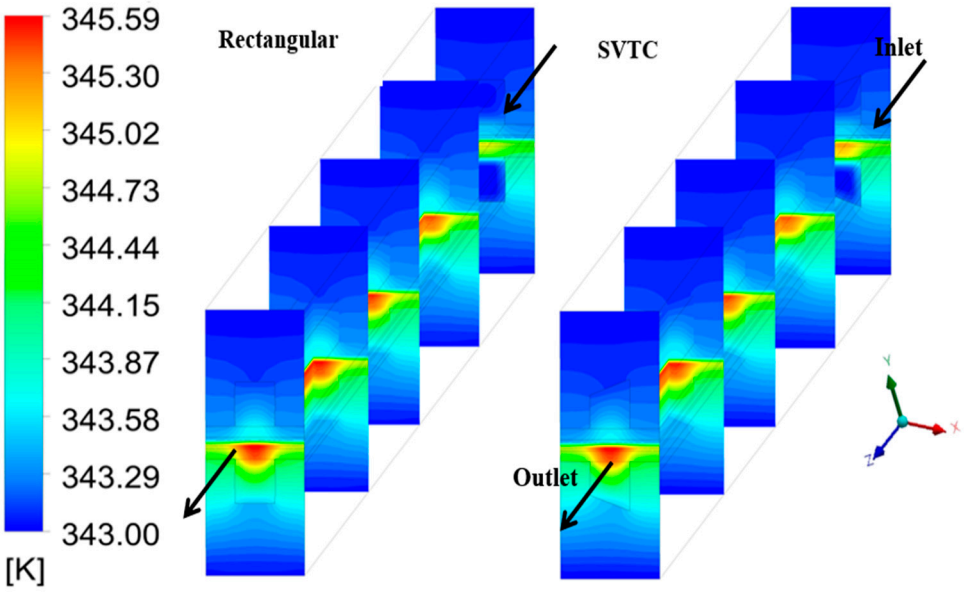


Figure 9. Comparative temperature distribution in PEMFC for rectangular and SVTC designs.

Figure 10 displays the pressure distribution within the PEMFC for rectangular and SVTC designs. The SVTC configuration produces a slightly higher pressure drop due to the tapered sidewalls, which accelerate gas flow and improve reactant convection along the channel. This promotes more uniform gas distribution and effective water removal, while the rectangular channel shows lower flow momentum and less efficient mass transfer.

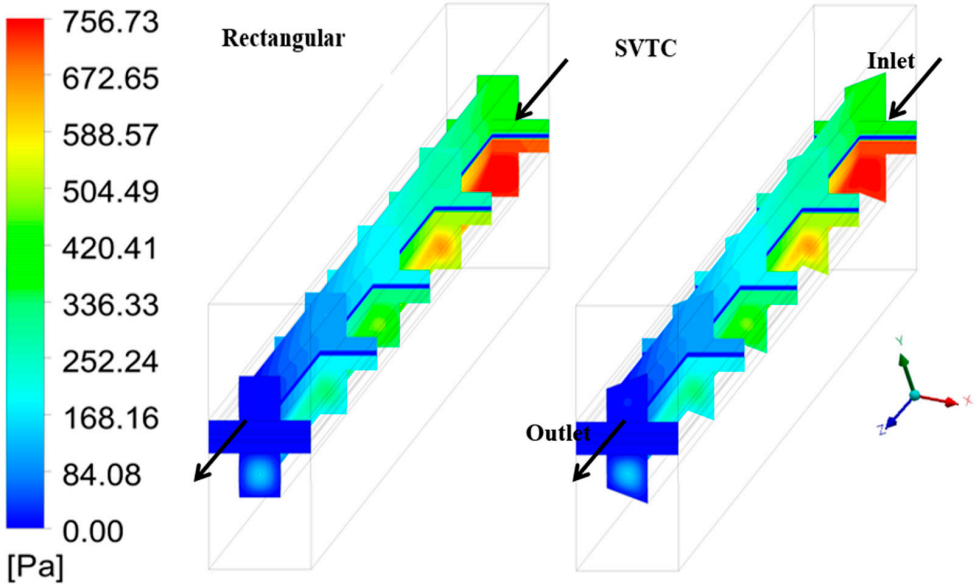


Figure 10. Comparative pressure distribution in PEMFC for rectangular and SVTC designs.

3.2. Analysis of Polarization, Power Density, and Pressure Drop

Figure 11 shows that all SVTC channel configurations exhibit a similar voltage current density trend, with voltage rising to a peak before declining. Peak performance occurs near 0.88 A/cm^2, where configuration R1 reaches 0.8822 A/cm^2 and R5 records 0.8794 A/cm^2. Although R5 has a slightly lower current density, it demonstrates better electrochemical performance. This improvement is likely attributed to enhanced reactant distribution, lower mass transport resistance, and more effective water removal resulting from the SVTC channel geometry.

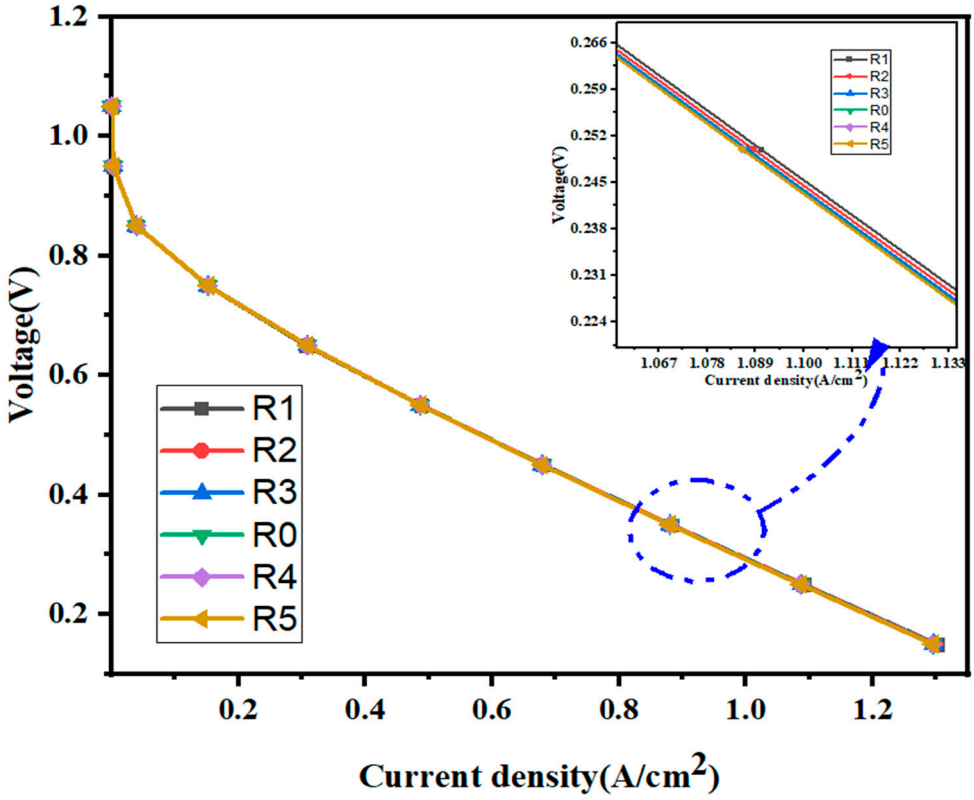


Figure 11. Polarization curves for different taper ratio configurations of SVTC channels.

Figure 12 presents the power density characteristics for SVTC channel configurations with varying taper ratios. All designs exhibit a similar pattern, where power density increases with current density until reaching a maximum. Configuration R1 records the highest peak power density at 0.30877 W/cm^2, indicating the most efficient performance among the tested designs. R5 follows closely with a peak of 0.30779 W/cm^2. Despite the small difference, R5's result highlights the beneficial influence of tapering in improving flow distribution, reducing transport losses, and enhancing water removal.

Figures 13 and 14 present the effect of taper ratio on output power density and total pressure drop in SVTC channels. As illustrated in Figure 13, the output power density shows only slight variation across all configurations, ranging between 0.30779 and 0.30877 W/cm^2. These minor differences indicate that tapering exerts little influence on the gross electrochemical output of the system.

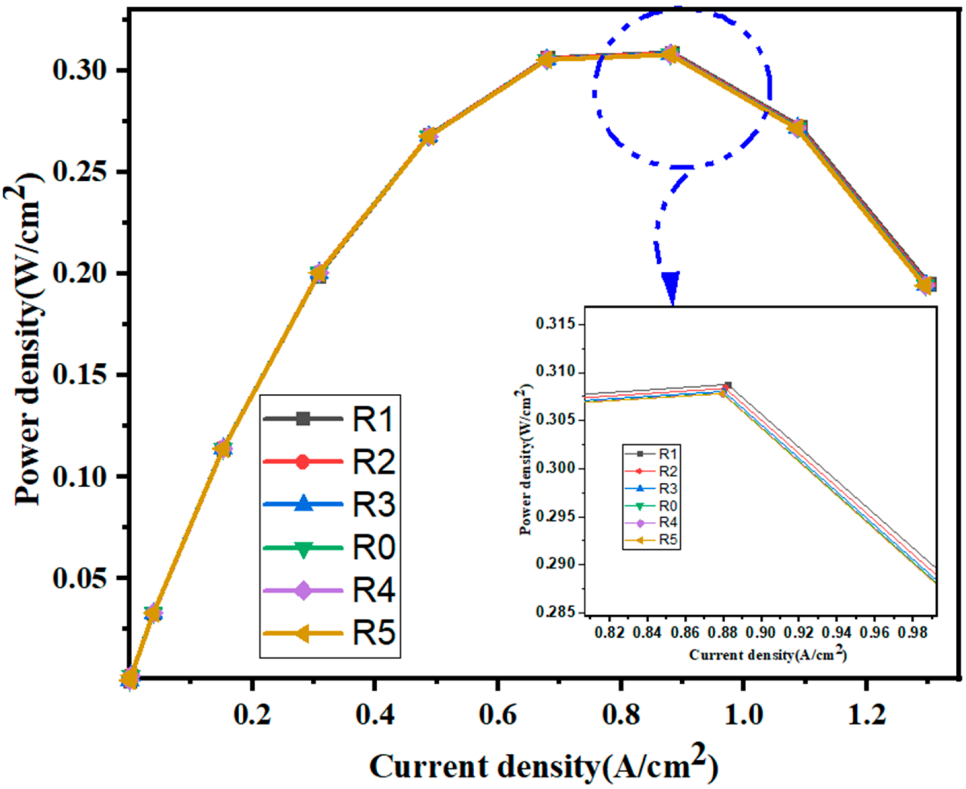


Figure 12. Power density characteristics for different taper ratio configurations of SVTC channels.

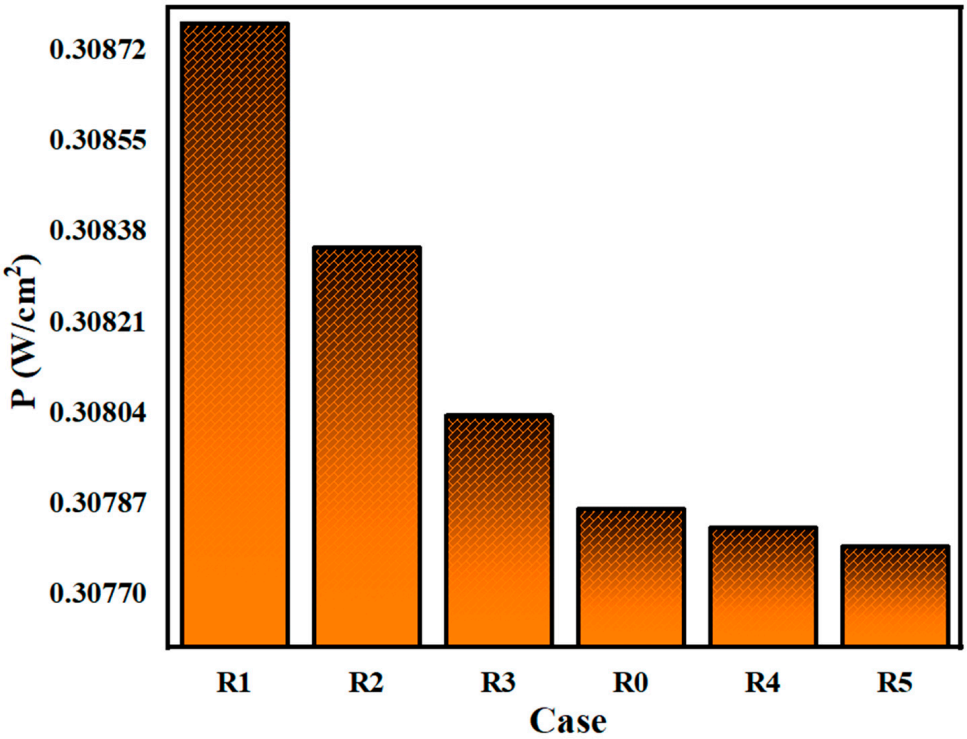


Figure 13. Comparison of output power density characteristics for different taper ratio configurations of SVTC channels.

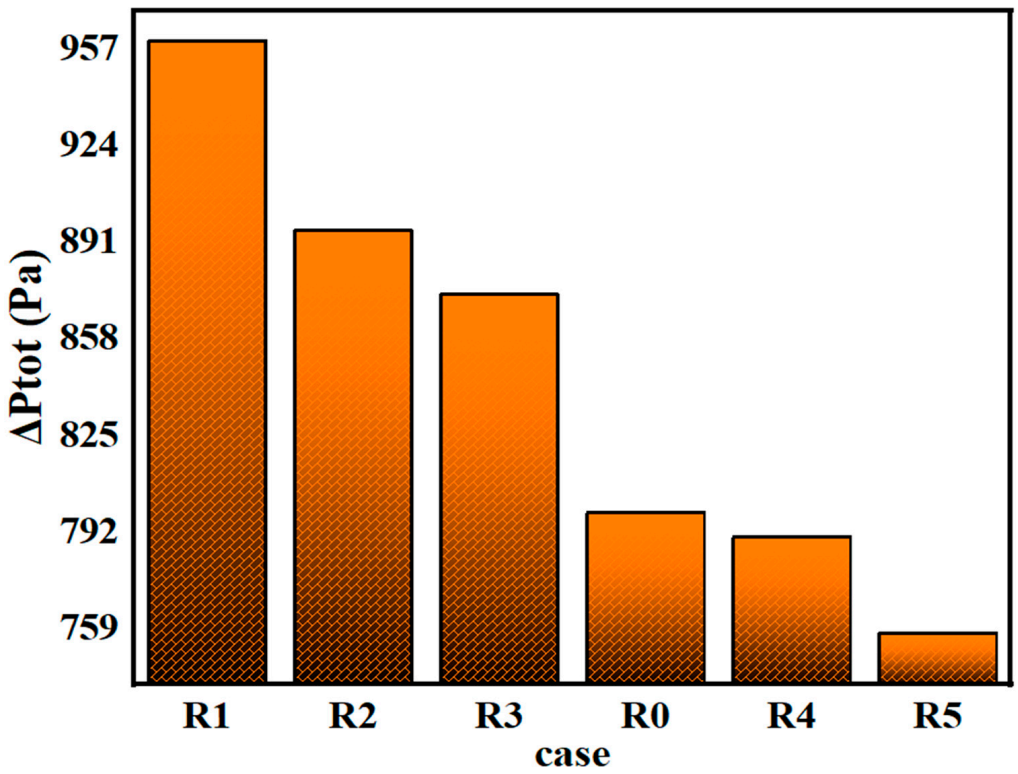


Figure 14. Comparison of total pressure drop characteristics for different taper ratio configurations of SVTC channels.

It is important to note that the total pressure drop is computed as the difference between the area-weighted inlet and outlet pressures:

$$\Delta P_{tot} = P_{inlet} - P_{outlet} \quad (14)$$

By contrast, Figure 14 demonstrates a clear dependence of pressure drop on taper ratio. The total pressure drops decreases progressively with increasing taper, from 959.77 Pa in case R1 to 757.68 Pa in case R5. This reduction in hydraulic resistance lowers the pumping power demand, which in turn enhances the net power density, as summarized in Table 3. Notably, the net power density increases from 0.294558 W/cm^2 in R1 to a peak of 0.297031 W/cm^2 in R5.

Table 3. Influence of SVTC ratio on pressure drop, output, and net power density.

Case	Total p.	Power Density Output W (W/cm^2)	Pumping Power Density W (W/cm^2)	Net Power Density W (W/cm^2)
R1	959.77	0.30877	0.014212	0.294558
R2	895.00	0.30835	0.013196	0.295154
R3	873.26	0.308035	0.012750	0.295285
R0	798.78	0.30786	0.011534	0.296326
R4	790.46	0.307825	0.011383	0.296442
R5	757.68	0.30779	0.010759	0.297031

These results underline the significance of flow field geometry optimization. While taper ratio has little effect on gross power output, it strongly affects fluid dynamics and associated energy losses. Greater tapering, as seen in R4 and R5, promotes improved reactant distribution, facilitates water removal, and reduces transport resistance, leading to

higher overall system efficiency. Thus, minimizing pressure drop emerges as a key strategy for maximizing the net performance of PEM fuel cells.

Table 3 shows how the taper ratio affects flow behavior and overall energy efficiency in SVTC channels. Although the power density output stays nearly the same across all cases, a lower taper ratio leads to a noticeable drop in both pressure loss and the power needed for pumping. As a result, the net power density increases steadily, with R5 reaching the highest value of 0.297031 W/cm^2. This suggests that more tapered channels help improve the distribution of reactants and remove excess water more effectively, while also lowering flow resistance. On the other hand, less tapered (more rectangular) channels reduce pressure drop but may limit reactant transport. Balancing these effects is important, as the design of the flow field is a pivotal aspect of PEMFC optimization, with the taper ratio emerging as a key geometric variable. This parameter critically influences the trade-off between efficient reactant distribution and the minimization of parasitic energy losses. In the subsequent part of this study, a comprehensive evaluation of the numerical findings is provided, exploring their consequences for overall cell efficacy and outlining the principal insights obtained from the computational analysis.

Consequently, the taper ratio is instrumental in augmenting PEMFC functionality through its regulation of mass transport phenomena and associated energy consumption. For clarity, this segment can be structured using subheadings to deliver a focused and accurate summary of the computational outcomes, their analysis, and the ensuing deductions.

4. Conclusions

In this study, a three-dimensional computational model was used to examine how different gas channel geometries affect the performance of a single-channel PEMFC. A computational analysis was conducted to evaluate a conventional rectangular channel against a SVTC, utilizing the ANSYS FLUENT software under steady-state and isothermal conditions.

The simulation results demonstrated that the SVTC configuration enhances fuel cell performance through improved reactant distribution and more effective water management, coupled with a reduction in pressure drop. These combined effects contributed to superior voltage stability and a marked improvement in power density relative to the conventional rectangular design. Out of all the tested taper ratios, the R5 configuration delivered the best performance, with the highest net power density of 0.297031 W/cm^2 due to its efficient flow characteristics and reduced pumping power.

These findings demonstrate that channel geometry, specifically the taper ratio, has a strong impact on both transport behavior and overall efficiency. Optimizing this aspect of the flow field can lead to substantial gains in PEMFC operational performance and offers critical insights for advancing flow field architectures.

While the proposed SVTC design offers significant performance improvements in PEMFCs, it is crucial to consider the engineering application value and manufacturing feasibility of this innovative geometry.

Furthermore, the potential risks of stress concentration in metal bipolar plates, introduced by the tapered channels, were also addressed. Such stress concentrations have the potential to threaten the operational lifespan of the bipolar plates, thereby warranting dedicated studies to assess their implications for the long-term functional reliability of PEMFC systems.

Author Contributions: Conceptualization, M.E.A.G., A.C., F.K. and A.M.; Methodology, M.E.A.G. and A.M.; Software, M.E.A.G. and A.M.; Validation, M.E.A.G., A.C. and A.M.; Formal analysis, M.E.A.G.; Investigation, M.E.A.G., A.C., F.K., A.M. and A.Z.; Resources, M.E.A.G., F.K. and A.Z.;

Data curation, M.E.A.G.; Writing—original draft, M.E.A.G.; Writing—review & editing, A.C., F.K., A.M., A.Z. and N.L.; Visualization, A.C., F.K., A.M., A.Z. and N.L.; Supervision, A.C., F.K. and N.L.; Project administration, A.C. All authors have read and agreed to the published version of the manuscript.

Funding: This research received no external funding.

Institutional Review Board Statement: Not applicable.

Informed Consent Statement: Not applicable.

Data Availability Statement: The original contributions presented in this study are included in the article. Further inquiries can be directed to the corresponding author.

Conflicts of Interest: The authors declare no conflict of interest.

Abbreviations

Symbols

A	Water activity
D	Mass diffusion coefficient, m/s
F	Faraday constant, C/mol
H	Channel height, mm
h	Enthalpy, W/ m^2 .C
I	improvement,
J	Exchange current density, A/m^2
K	Permeability, m^2
k	Thermal conductivity, W/m. K
L	Channel length, mm
M	Molecular weight, g/mol
P	Pressure, Pa
R	Universal gas constant, J/mol. K
T	Temperature, K
V_{oc}	Open circuit voltage, V
W	Channel width, mm
y	Mass fraction,

Greek symbols

α	Water transfer coefficient,
γ	Concentration coefficient,
ε	Porosity,
η	Overpotential, V
λ	Water content
μ	Viscosity, kg/m. s
ρ	Density, kg/m^3
σ	Conductivity, 1/ohm. M
φ	Potential, V

Subscripts and superscripts

An	Anode
BICGSTAB	Biconjugate Gradient Stabilize Method
Cat	Cathode
Cell	Fuel cell
CFD	Computational fluid dynamic
CL	Catalyst Layer
F-cycle	Full Approximation Scheme

eff	Effective
GDL	Gas diffusion layer
MEA	Membrane electrolyte assembly
mem	Membrane
PEMFC	Proton Exchange Membrane Fuel Cell
Ref	Reference value
Rel	Relative
Sol	Solid
SVTC	Symmetric V-Tapered Cross-Section

References

1. Shah, S.V.; Lamba, B.Y.; Tiwari, A.K.; Chen, W.H. Sustainable biogas production via anaerobic digestion with focus on CSTR technology: A review. *J. Taiwan Inst. Chem. Eng.* **2024**, *162*, 105575. [CrossRef]
2. Zhang, J. Energy access challenge and the role of fossil fuels in meeting electricity demand: Promoting renewable energy capacity for sustainable development. *Geosci. Front.* **2024**, *15*, 101873. [CrossRef]
3. Wang, L.; Zhou, T.; Hou, B.; Yang, H.; Hu, N.; Zhang, M. A Comprehensive Review of Biomass Gasification Characteristics in Fluidized Bed Reactors: Progress, Challenges, and Future Directions. *Fluids* **2025**, *10*, 147. [CrossRef]
4. Algburi, S.; Al-Dulaimi, O.; Fakhruldeen, H.F.; Khalaf, D.H.; Hanoon, R.N.; Jabbar, F.I.; Hassan, Q.; Al-Jiboory, A.K.; Kiconco, S. The green hydrogen role in the global energy transformations. *Renew. Sustain. Energy Transit.* **2025**, *8*, 100118. [CrossRef]
5. Li, X.; Ye, T.; Meng, X.; He, D.; Li, L.; Song, K.; Jiang, J.; Sun, C. Advances in the Application of Sulfonated Poly (Ether Ether Ketone) (SPEEK) and Its Organic Composite Membranes for Proton Exchange Membrane Fuel Cells (PEMFCs). *Polymers* **2024**, *16*, 2840. [CrossRef]
6. Lei, H.; Deng, C.; Li, X.; Liu, Z.; Yang, S. Performance improvement of PEMFC by employing bionic flow channel. *Sustain. Futures* **2025**, *9*, 100613. [CrossRef]
7. Wang, C.; Yu, Z.; Liu, W.; Qiao, Y.; Wang, D.; Cui, B.; Gao, H. Performance improvement for proton exchange membrane fuel cells (PEMFCs) with different parallel flow fields by optimizing ribs arrangement. *Energy* **2025**, *322*, 135585. [CrossRef]
8. Liu, K.; Liu, Y.; Han, Q.; Pei, P.; Zhang, L.; Sun, H. Enhancing PEMFC performance through dome-like variable cross-section channels: A study on mass transfer and power density optimization. *Int. J. Electrochem. Sci.* **2025**, *20*, 100920. [CrossRef]
9. Kumar, A.; Reddy, R.G. Effect of gas flow-field design in the bipolar/end plates on the steady and transient state performance of polymer electrolyte membrane fuel cells. *J. Power Sources* **2006**, *155*, 264–271. [CrossRef]
10. Kuo, J.K. The effects of buoyancy on the performance of a PEM fuel cell with a wave-like gas flow channel design by numerical investigation. *Int. J. Heat Mass Transf.* **2007**, *50*, 4166–4179. [CrossRef]
11. Kloess, J.P.; Wang, X.; Liu, J.; Shi, Z.; Guessous, L. Investigation of bio-inspired flow channel designs for bipolar plates in proton exchange membrane fuel cells. *J. Power Sources* **2009**, *188*, 132–140. [CrossRef]
12. Xiao, F.; Chen, T.; Lan, Y.; Chen, Z. Flow field design and parameter optimization of PEMFC based on leaf vein structure. *Renew. Energy* **2025**, *241*, 122317. [CrossRef]
13. Bulgarini, M.; Piegari, L.; Veneri, O. Computational Fluid Dynamic Investigation of Local Flow-Field Geometry on PEM Fuel Cell Performance. *Energies* **2024**, *17*, 3643. [CrossRef]
14. Chowdhury, P.R.; El-Bakary, M.A.; Nada, S.A. Design of Flow Fields for High-Temperature PEM Fuel Cells. *Energies* **2024**, *17*, 4898. [CrossRef]
15. Rostami, L.; Haghshenasfard, M.; Sadeghi, M.; Zhiani, M. Numerical Investigation of Flow Channel Design and Tapered Slope Effects in PEM Fuel Cells. *Sustainability* **2022**, *14*, 11167. [CrossRef]
16. Hawkins, E.K.; Cheng, J.S.; Abbate, J.A.; Pilegard, T.; Stellmach, S.; Julien, K.; Aurnou, J.M. Laboratory models of planetary core-style convective turbulence. *Fluids* **2023**, *8*, 106. [CrossRef]
17. Besagni, G.; Varallo, N.; Mereu, R. Computational fluid dynamics modelling of two-phase bubble columns: A comprehensive review. *Fluids* **2023**, *8*, 91. [CrossRef]
18. Jeong, S.J.; Lee, S.J.; Moon, S.J. CFD thermo-hydraulic evaluation of a liquid hydrogen storage tank with different insulation thickness in a small-scale hydrogen liquefier. *Fluids* **2023**, *8*, 239. [CrossRef]
19. Dehghanghadikolaei, A.; Abdul Halim, B.; Khoshbakhtnejad, E.; Sojoudi, H. Dynamics of a water droplet impacting an ultrathin layer of oil suspended on a pool of water. *Fluids* **2024**, *9*, 82. [CrossRef]
20. Fagbade, A.; Heinz, S. Continuous eddy simulation vs. resolution-imposing simulation methods for turbulent flows. *Fluids* **2024**, *9*, 22. [CrossRef]
21. Fahim, K.H.; Dhahad, E.M.A.H.A. Effect of Geometric Design of the Flow Fields Plat on the Performance of A PEM Fuel Cell: A Review. *Int. J. Sci. Eng. Res.* **2017**, *8*, 25.

22. Carcadea, E.; Ismail, M.S.; Ingham, D.B.; Patularu, L.; Schitea, D.; Marinoiu, A.; Ion-Ebrasu, D.; Mocanu, D.; Varlam, M. Effects of geometrical dimensions of flow channels of a large-active-area PEM fuel cell: A CFD study. *Int. J. Hydrogen Energy* **2021**, *46*, 13572–13582. [CrossRef]
23. Rostami, L.; Haghshenasfard, M.; Sadeghi, M.; Zhiani, M. A 3D CFD model of novel flow channel design based on the serpentine and the parallel design for performance enhancement of PEMFC. *Energy* **2022**, *258*, 124726. [CrossRef]
24. Sun, F.; Su, D.; Li, P.; Dong, X. A novel 3D fine-mesh flow field design and performance analysis for proton exchange membrane fuel cells. *J. Power Sources* **2023**, *584*, 233572. [CrossRef]
25. Yuan, L.; Jin, Z.; Yang, P.; Yang, Y.; Wang, D.; Chen, X. Numerical analysis of the influence of different flow patterns on power and reactant transmission in tubular-shaped pemfc. *Energies* **2021**, *14*, 2127. [CrossRef]
26. Elaibi, A.M. A Performance Study of Fuel Cells with Novel Channel Cross-Section Configuration. *Vital Annex. Int. J. Nov. Res. Adv. Sci.* **2025**, *4*, 129–138.
27. Wang, H.; Fang, H.; Guo, J.; Lin, Y. Design and optimization of variable cross-section wave flow channels in proton exchange membrane fuel cells based on physical field. *Int. J. Green Energy* **2025**, 1–19.–19. [CrossRef]
28. Kaplan, M. Numerical investigation of influence of cross-sectional dimensions of flow channels on PEM fuel cell performance. *J. Energy Syst.* **2021**, *5*, 137–148. [CrossRef]
29. Suvanjumrat, C.; Seanglumlert, C.; Sripongpun, J.; Permpol, T.; Priyadumkol, J.; Boekfah, A.; Kanokmedhakul, Y.; Promtong, M.; Punurai, W. Investigation of Cross-Sectional Aspect Ratios in Straight Flow Channels on PEMFC Performance Using OpenFOAM. In Proceedings of the International Conference on Renewable and Clean Energy, Fukuoka, Japan, 15–17 February 2025; Springer: Singapore, 2025; pp. 39–46. [CrossRef]
30. Wu, Y.; Li, Y.; Chen, H.; Zhang, X.; Zhang, X.; Ma, C. Numerical Investigation of Proton Exchange Membrane Fuel Cell Performance Based on Different Flow Channel Cross-sectional Designs. In Proceedings of the 2025 IEEE International Conference on Electronics, Energy Systems and Power Engineering (EESPE), Tianjin, China, 12–14 September 2025; IEEE: Piscataway, NJ, USA, 2025; pp. 94–98. [CrossRef]
31. ANSYS Inc. *ANSYS Fluent 18.1 Fuel Cell Modules Tutorial Guide*; ANSYS Inc.: Canonsburg, PA, USA, 2017.
32. Springer, T.E.; Zawodzinski, T.A.; Gottesfeld, S. Polymer electrolyte fuel cell model. *J. Electrochem. Soc.* **1991**, *138*, 2334. [CrossRef]
33. Ticianelli, E.A.; Derouin, C.R.; Srinivasan, S. Localization of platinum in low catalyst loading electrodes to to attain high power densities in SPE fuel cells. *J. Electroanal. Chem. Interfacial Electrochem.* **1988**, *251*, 275–295. [CrossRef]
34. Mohammedi, A.; Sahli, Y.; Moussa, H.B. Optimization study of the produced electric power by planar PEMFC-SCG. *Renewable Energy Focus* **2020**, *35*, 72–83. [CrossRef]
35. Mohammedi, A.; Sahli, Y.; Moussa, H.B. 3D investigation of the channel cross-section configuration effect on the power delivered by PEMFCs with straight channels. *Fuel* **2020**, *263*, 116713. [CrossRef]

Disclaimer/Publisher's Note: The statements, opinions and data contained in all publications are solely those of the individual author(s) and contributor(s) and not of MDPI and/or the editor(s). MDPI and/or the editor(s) disclaim responsibility for any injury to people or property resulting from any ideas, methods, instructions or products referred to in the content.